

Investigation of the Galvanic Mechanism for Localized Carbon Dioxide Corrosion Propagation Using the Artificial Pit Technique

J. Han,* B.N. Brown,** and S. Nešić†,***

ABSTRACT

Localized carbon dioxide (CO_2) corrosion is the most dangerous type of internal corrosion to mild steel pipelines in the oil and gas industry since the penetration rate of localized corrosion can be one or more magnitudes higher than that of uniform corrosion. In this study, the focus is on propagation of localized CO_2 corrosion on mild steel that occurs by a galvanic mechanism. A galvanic cell is established by the coupling of two distinct areas in a conductive CO_2 solution: a bare steel surface and an iron carbonate (FeCO_3) layer-covered steel surface. It was found that localized CO_2 corrosion propagates when a stable difference in corrosion potential is established between the anode (bare steel surface) and the cathode (FeCO_3 -covered surface). Stable propagation will occur only when the conditions are in the "gray zone," i.e., close to saturation with respect to FeCO_3 , when no significant FeCO_3 dissolution nor precipitation is expected. Practically, this corresponds to when FeCO_3 supersaturation ($\text{SS}_{\text{FeCO}_3}$) is in the range from 0.5 to 2. The key environmental factors that affect propagation of localized CO_2 corrosion of mild steel are temperature, pH, partial pressure of CO_2 , salt concentration, and flow velocity. A protective FeCO_3 layer forms at high temperature ($>50^\circ\text{C}$); therefore, the galvanic mechanism of localized corrosion is valid only in this range. pH needs to be such that moderately protective FeCO_3 layers form, typically at pH 5.5 to

6.5. Critical partial pressures of CO_2 is around 0.1 bar to 2 bar, above this very protective FeCO_3 films form at high temperature, giving a very low likelihood of localized attack. The solubility of FeCO_3 increases with increasing salt concentration, making it more difficult to form protective FeCO_3 layers and more likely to get localized corrosion propagation. Turbulent flow assists localized corrosion propagation by sweeping away corrosion products from the rapidly corroding steel surface and thereby preventing reformation of the protective FeCO_3 layer.

KEY WORDS: carbon dioxide corrosion, environmental factors, galvanic cell, localized corrosion, pit geometry, propagation

INTRODUCTION

Localized carbon dioxide (CO_2) corrosion is the most dangerous type of internal corrosion of mild steel pipelines seen in the oil and gas industry. The penetration rate of localized corrosion can be one or more magnitudes higher than that of uniform corrosion. This process has been observed frequently in the field and was widely studied in the past.¹⁻³³

A number of environmental factors have been associated with the onset of localized corrosion of mild steel pipelines. These include poor corrosion inhibition, local water separation in oil-water flow, differential condensation in wet gas flow, and flow disturbances such as weld beads, flanges, the presence of bacteria, solids, organic acids, hydrogen sulfide, etc. However, a comprehensive mechanism of "pure" localized CO_2 corrosion of mild steel, even without these complicating factors is still not well defined.

Localized corrosion mechanism scenarios "borrowed" from other mild steel and passive metal pit-

Submitted for publication May 20, 2009; in revised form, May 13, 2010. Part of this paper was presented as paper no. 07323 at CORROSION/2007, March 2007, Nashville, TN.

† Corresponding author. E-mail: nesic@ohio.edu.

* Institute for Corrosion and Multiphase Technology, Department of Chemical and Biomolecular Engineering, Ohio University, 342 West State St., Athens, OH 45701. Present address: Earth Systems Observations (EES-14), Earth and Environmental Sciences Division (EES), Los Alamos National Laboratory, Los Alamos, NM.

** Institute for Corrosion and Multiphase Technology, Department of Chemical and Biomolecular Engineering, Ohio University, 342 West State St., Athens, OH 45701.

ting studies, which have been invoked repeatedly in the past trying to explain localized CO_2 corrosion, including differential aeration,³⁴ pit acidification,³⁵ and point defect mechanism,³⁶⁻³⁷ do not apply. Differential aeration cannot be considered for obvious reasons, because most CO_2 systems are oxygen-free. The mechanism of pit acidification does not seem to hold because of the strong buffering capacity of CO_2 solutions, i.e., pH changes are much more difficult to achieve in this case, particularly the large changes needed to explain the pit acidification theory. Furthermore, pit acidification is usually related to the formation of ferric oxides and hydroxides, which are not seen in CO_2 corrosion due to the absence of oxygen. The point defect mechanism valid for passive metals does not apply either since the nature of localized CO_2 corrosion of mild steel is rather different to the one seen when mild steel passivates in neutral or alkaline solutions. This type of attack is usually qualified as “mesa attack” (Figure 1), including large receded areas free of corrosion products that have corroded severely, sharply divided from surrounding protected areas covered with a corrosion product. The name “mesa” is borrowed from the same term used to describe well-known geologic formations.

Another overlapping term, which can be found in the literature for this type of attack, is “flow-induced localized corrosion” or FILC.¹⁰⁻¹⁷ The name implies that the type of attack is related to the corrosion product film being locally removed by flow, causing the metal to be exposed directly to the corrosive environment. While this is a plausible explanation for localized corrosion initiation, it cannot explain the process of localized attack propagation. If film removal by flow was the full explanation, localized CO_2 corrosion of mild steel would not be any more severe than that of bare steel corrosion at any given set of conditions—in reality, it is. Furthermore, this type of localized corrosion is observed under very mild flow conditions and even in stagnant solutions;¹⁸ therefore, additional explanation is required.

Nyborg and Dugstad²¹⁻²⁴ reported observations of localized corrosion initiation using an optical imaging technique. According to them, given the right set of conditions (involving specific water chemistry and flow), localized corrosion initiates underneath a corrosion product layer made up predominantly from iron carbonate (FeCO_3). Larger pits form by merging with neighboring pits. The unsupported “covers” of the pits made up from the corrosion product layer are removed by flow turbulence, exposing the bare steel to an aggressive environment, leading to localized corrosion propagation. A hypothesis was made about the galvanic nature of the localized corrosion propagation process, without any further elaboration.

Actually, the galvanic mechanism was often invoked in connection with localized CO_2 corrosion propagation in the past.^{3-6,8,19-20,21-24} For example,



FIGURE 1. Section of a corroded pipe showing localized attack. Image source ConocoPhillips, with permission.

Achour,⁸ based on his own observations, arbitrarily assumed a potential difference between the protected and unprotected areas to be 100 mV. While this is possible, there are no studies that have clearly provided evidence in support of the apparent galvanic mechanism of localized CO_2 corrosion propagation. This is the subject of the present study.

In this study, propagation of localized corrosion is hypothesized to occur when a galvanic cell is established by coupling two distinct areas, a bare steel surface (acting as an anode) and an FeCO_3 layer-covered steel surface (acting as a cathode), in a conductive CO_2 solution. It should be noted that in the present work, the discussion will not be focused on mechanisms leading to localized attack initiation since there seems to be consensus that this happens when portions of the protective FeCO_3 film are removed from the steel surface by chemical or mechanical means.

In the present work, an attempt will be made to answer two basic questions:

—What is the mechanism of the accelerated localized corrosion propagation on mild steel in CO_2 solutions?

—Which are the key factors that influence it?

To answer these questions, an artificial pit experimental setup was developed, as described below, which was inspired primarily by the previously published “pencil pit”³⁸ and “artificial pit”³⁹ designs. Similar experimental designs were used previously for investigation of localized corrosion and under deposit corrosion where a galvanic mechanism is plausible.⁴⁰⁻⁴³ Marsh, et al.,³⁹ and Turnbull, et al.,³⁸ designed an artificial pit (or “pencil pit” as it was called in the first publication³⁸) to investigate the effect of inhibitors on localized corrosion. In their designs, the anode and cathode were isolated from each other to measure galvanic coupling, resulting in localized corrosion. The two electrodes were physically separated: in Marsh’s,

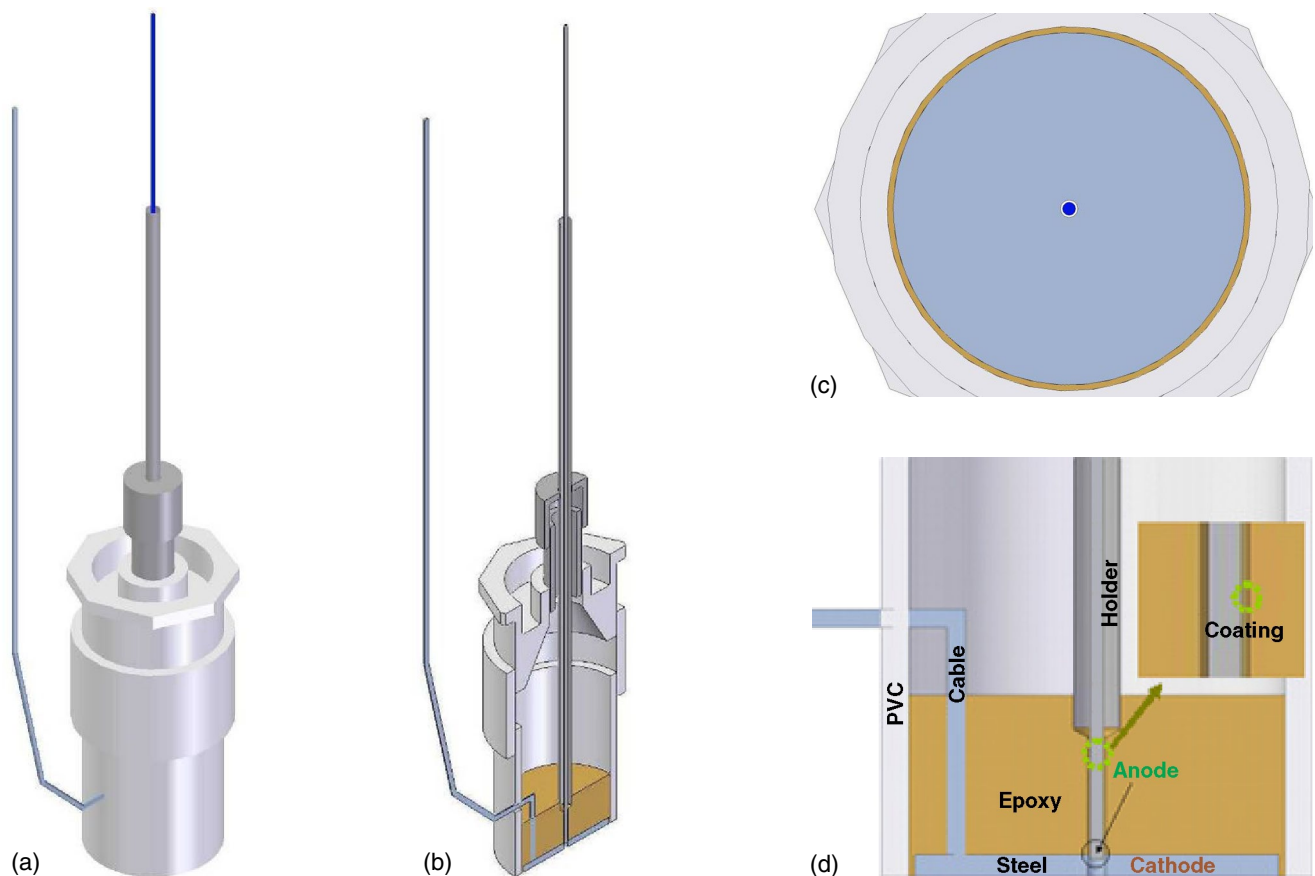


FIGURE 2. (a) Fully assembled artificial pit, (b) cutaway side view, (c) enlarged bottom view of cathode; center hole for anode, and (d) detailed cross section view.

et al.,³⁹ case—within a single cell; in Turnbull's, et al.,³⁸ case—between two glass cells connected with a salt bridge. The latter made it easier to control the separate aqueous environments, but also introduced experimental problems; namely, it is difficult to ensure exactly the same corrosive environment for the anode and cathode when in two different cells. In both studies, the most serious drawback was related to the physical separation distance of the anode and cathode. This gives rise to ohmic resistance in the aqueous phase during any galvanic current measurements. In reality, the anode and cathode are part of the same steel substrate in very close proximity; this was the first modification that was better accounted for in the new artificial pit design. The present design is referred to below as the “artificial pit” (AP).

EXPERIMENTAL DESIGN

Artificial Pit Design

The goal of the new AP technique was to simulate a localized corrosion geometry including open pits (both receded and shallow) as well as occluded pits, using in situ measurements. The design of the new AP is shown in Figure 2, the main features being:

- The cathode is a 16-cm² round, flat surface, which is approximately 1,000 times larger than the 0.018-cm² anode.
 - The cathode and anode are electronically insulated from each other by a ca. 1-mm-thick polyvinyl chloride (PVC) coating on the anode's outer wall. This prevents short-circuiting by direct contact between the anode's outer wall and the cathode's inner wall in the solution while keeping them as close as possible.
 - The anode and cathode are externally connected by a zero-resistance ammeter (ZRA). This mimics reality where the pit bottom is directly connected to the surrounding steel surface.
 - The depth of the anode is adjustable. This allows investigation of pit behavior at different pit depths in different scenarios of pit propagation.
 - All parts of the artificial pit are tightly compacted into one unit. The environment for the anode and cathode is similar since they are located in the same glass cell.
- As shown in the design of the artificial pit, the coupling current (galvanic current) and the mixed

potential (galvanic potential) can be monitored while the anode and cathode are connected externally via a ZRA. The electrochemical characteristics for the disconnected anode and cathode can also be measured by available techniques including linear polarization resistance (LPR) at a sweep rate of 0.2 mV/s within ± 5 mV vs. open-circuit potential (OCP) and electrochemical impedance spectroscopy (EIS) at frequency range of 0.1 Hz to 100 kHz, etc.

Corrosion Cell Setup

The overall AP glass cell test setup is depicted in Figure 3. A classical three-electrode electrochemical arrangement is used, including mild steel working electrodes (C1008 [UNS G10080]⁽¹⁾ was used for both the anode and cathode), a platinum wire counter electrode, and an external saturated silver/silver chloride (Ag/AgCl) reference electrode connected with the cell by using a Luggin capillary and a potassium chloride (KCl) salt bridge.

Experimental Procedures

Two steel surfaces, serving as cathode and anode, were polished using 200-, 400-, and 600-grit sand paper in sequence. Each was wetted with 2-propanol to prevent the surface from overheating during polishing. Specimen surfaces were ultrasonicated in 2-propanol solvent to remove polishing debris, and then dried with a cool air blow. The cathode was placed in an empty glass cell under a dry CO₂ gas environment, while the anode was preserved in a desiccator.

An aqueous sodium chloride (NaCl) solution was first deaerated with CO₂ and heated to 80°C in another auxiliary glass cell. The pH was adjusted to 6.6 by adding a deaerated 1 M sodium bicarbonate (NaHCO₃) solution. CO₂ purging continued an additional half hour after the addition of NaHCO₃ solution to ensure the best possible deaeration of the solution.

After the solution was prepared in the auxiliary glass cell, the cathode was then submerged in the electrolyte by pumping the prepared solution across. A deaerated, dilute iron(II) chloride (FeCl₂) solution was injected into the solution to achieve a high ferrous ion (Fe²⁺) concentration and a FeCO₃ supersaturation (SS_{FeCO₃}) of about 300 at the beginning of the experiment (actual concentration of Fe²⁺ was about 50 ppm), which is required for rapid formation of a corrosion product layer. Typically, in less than 2 days of corrosion in such an environment, a reproducible, protective FeCO₃ film was developed on the cathode, as the bulk Fe²⁺ concentration decreased to 1 ppm to 2 ppm due to precipitation. Combined LPR and EIS techniques were used to measure the general corrosion rate during the FeCO₃ layer formation process. When the corrosion rate became stable and was less

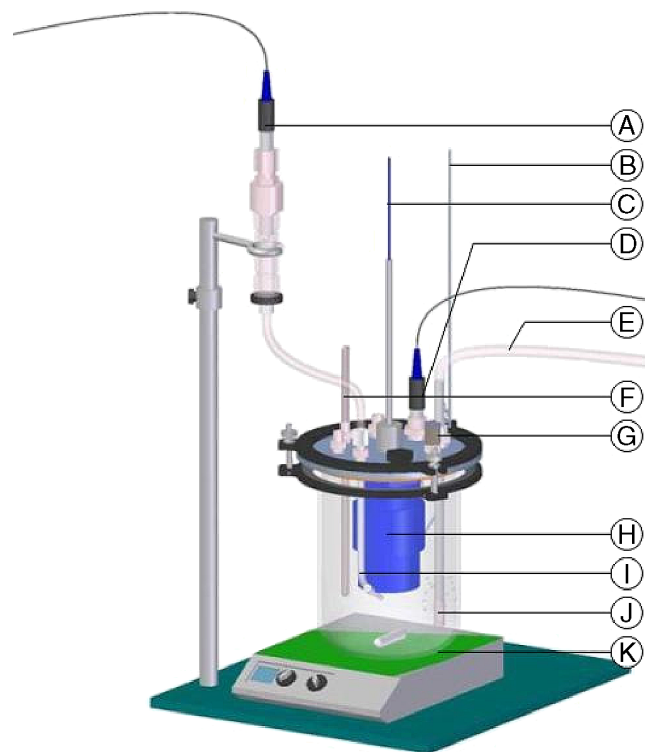


FIGURE 3. Glass cell arrangement for the artificial pit test cell. A—Ag/AgCl reference electrode, B—wire connection to cathode, C—wire connection to anode, D—pH probe, E—gas inflow, F—thermocouple probe, G—gas outflow, H—artificial pit device, I—Luggin capillary tube, J—gas dispersion tube, K—hot plate/stirrer.

than 0.1 mm/y, the FeCO₃ layer formation process on the cathode was deemed complete.

Solution conditions were then adjusted for the following AP test. The pH was changed, if needed, by adding a deaerated 1-M NaHCO₃ or a dilute 0.01-M hydrochloric acid (HCl) solution based on the desired water chemistry. After that, the freshly polished anode wire surface was inserted into the small hole in the center of the cathode. The pit depth was adjusted with respect to the cathode surface by feeding the wire through a compression fitting.

The galvanic current between anode and cathode was recorded using a ZRA. The anode and cathode were disconnected occasionally for a very short period of time (<1 min) to measure OCP and corrosion rates using the LPR technique.

Test Matrix

The material used for the cathode and anode was mild steel C1008, and its chemical composition is listed in Table 1. The test matrix for artificial pit experiments is listed in Table 2. All the tests were carried out at 80°C. The CO₂ partial pressure for this atmospheric pressure glass cell system was about 0.5 bar at this temperature (the balance being water vapor pressure). The solution was stirred mildly by a magnetic stirring bar to achieve a uniform bulk solu-

⁽¹⁾ UNS numbers are listed in *Metals and Alloys in the Unified Numbering System*, published by the Society of Automotive Engineers (SAE International) and cosponsored by ASTM International.

TABLE 1
Chemical Composition of the Material (C1008) Used for the Anode and Cathode

Al	As	C	Co	Cr	Cu	Mn	Mo	Nb	Ni	P
0.030	0.004	0.060	0.004	0.033	0.130	0.400	0.017	0.001	0.048	0.010
S	Sb	Si	Sn	Ta	Ti	V	W	Zn	Zr	Fe
0.003	0.004	0.039	0.007	0.023	0.004	0.002	0.023	0.003	0.002	Balance

TABLE 2
Artificial Pit Test Matrix

General conditions	Material	C1008
	Temperature	80°C
	Partial pressure of CO ₂	0.53 bar
	Pit depth	<0.1 mm (shallow)
	Area ratio of cathode and anode	1,000:1
Cathode preparation	NaCl concentration	0.1, 1, 10 wt%
	Initial pH	6.6
	Initial ferrous iron concentration	50 ppm
	Stirring speed (stir-bar)	0 rpm
	Test period	1 to 2 days
Artificial pit test	Initial ferrous iron concentration	1 ppm to 2 ppm
	Adjusted pH	5.8 to 5.9, 6.6
	SS _{FeCO₃}	0.3 to 9
	NaCl concentration	0.1, 1, 10 wt%
	Stirring speed (stir-bar)	0, 400 rpm to 500 rpm
	Pit depth	<0.1 (shallow), 2 mm
Experiment duration	1 to 2 days	

tion mixing. The pH, FeCO₃ supersaturation, NaCl concentration, and stirring speed levels were adjusted to investigate their effects on localized corrosion propagation, as described below. The simulated pit geometry studied in this work included open shallow and receded pits, as well as occluded pits.

RESULTS AND DISCUSSION

Galvanic Mechanism of Localized CO₂ Corrosion Propagation

It was hypothesized above that the galvanic mechanism of localized corrosion propagation in a CO₂ environment is driven by an OCP difference between a mild steel surface covered with a protective FeCO₃ layer and a bare steel surface exposed to the same conditions. To test this hypothesis, it is important to determine whether the proposed scenario is borne out by measurements.

A typical scaling process, forming protective FeCO₃ on the cathode, is shown in Figure 4. During FeCO₃ formation, the general corrosion rate is reduced from the original value of approximately 1 mm/y, seen on a fresh bare steel surface, to approximately 0.1 mm/y on a FeCO₃-covered surface. Simultaneously, the OCP (corrosion potential) initially decreases and then increases. The difference between the OCP of the FeCO₃-covered surface at the end of the experiment

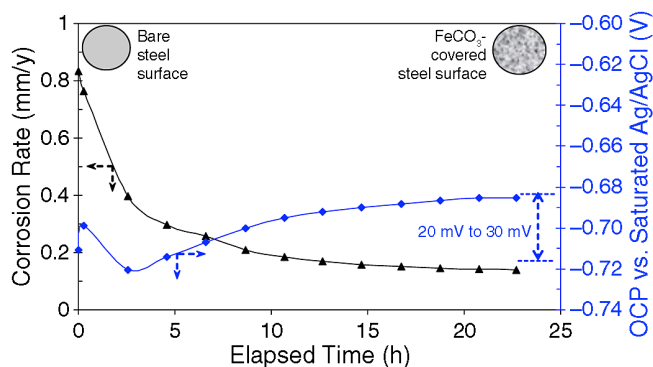


FIGURE 4. Corrosion rate and OCP with time for a typical protective FeCO₃ layer formation process on the cathode during an AP test at $T = 80^\circ\text{C}$, $\text{pH } 6.6$, $[\text{NaCl}] = 1 \text{ wt}\%$, $P_{\text{CO}_2} = 0.53 \text{ bar}$, $[\text{Fe}^{2+}]_{\text{initial}} = 50 \text{ ppm}$, stagnant.

and the bare steel surface at the beginning of the experiment is typically in the range from 20 mV to 30 mV under these test conditions. This observation indicates that a galvanic cell may be established between the bare and protected surfaces.

When a bare steel anode was inserted, and the anode and cathode were connected via a ZRA, the mixed potential was monitored continuously. In the same period the potential difference (galvanic potential) between the anode and cathode was measured by temporarily disconnecting the two. The data obtained

(Figure 5) show that when disconnected, the cathode OCP is consistently higher compared to the anode OCP. The coupled or mixed/galvanic potential lies between, and closer to, the cathode potential due to the much larger surface of the cathode, as would be expected from theory. Therefore, it is confirmed that the FeCO_3 -covered surface acts as a cathode, and the bare steel surface becomes an anode and a galvanic cell is established between these two surfaces. Since the FeCO_3 -covered cathode is much larger, the anode is polarized anodically and this should accelerate its corrosion rate.

Therefore, it is expected that the OCP difference measured between the anode and cathode drives a significant galvanic current. The coupled/galvanic current measured via a ZRA is shown in Figure 6 along with the OCP difference between the cathode and anode obtained in a disconnected mode. The solid rectangles represent the magnitude of the “driving force” (the OCP difference between disconnected anode and cathode) and the line shows the resulting galvanic current density as a function of time. It is obvious that when the driving force is large (i.e., OCP difference between anode and cathode is high), the galvanic current density is also high and vice versa. It should be noted that the current densities shown in Figure 6 are calculated based on the anode surface area. One can conclude that this represents explicit proof for the hypothesis stated above, that localized CO_2 corrosion propagates when a stable difference in corrosion potential is established between a larger-area mild steel surface covered by a protective FeCO_3 layer and a smaller-area bare steel surface corresponding to the bottom of a pit or a mesa corrosion surface.

Conditions Required for Steady, Localized CO_2 Corrosion Propagation

It has been known for some time that while localized corrosion of mild steel in a CO_2 environment initiates and propagates under certain conditions, in other cases it does not. For example, Videm and Dugstad³⁻⁴ observed localized corrosion in turbulent flow only when the solution was nearly or slightly saturated by FeCO_3 . Similar observations were reported by Nyborg and Dugstad,^{21,23-24} where they proposed a feasible temperature range being from 60°C to 90°C for localized corrosion to propagate. Achour, et al.,⁸ assumed that the pit propagation ceased when they were passivated due to FeCO_3 film formation. Sun, et al.,²⁵ followed this line of argument and generalized by stating that only if the corrosion condition fell into the so-called “gray zone,” the localized corrosion propagated.²⁷ The gray zone was defined as conditions constituting a solution that is close to saturation for FeCO_3 .

Therefore, it is possible to use the experimental tools and techniques discussed above and explicitly

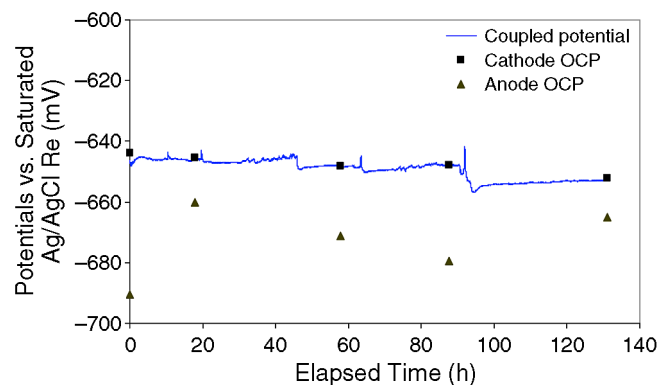


FIGURE 5. Disconnected OCP of anode and cathode and coupled (mixed) potential with time at $T = 80^\circ\text{C}$, $p_{\text{CO}_2} = 0.53$ bar, pH 5.9 to 6.1, $SS_{\text{FeCO}_3} = 0.3$ to 0.9, $[\text{NaCl}] = 1$ wt%, shallow pit, stagnant.

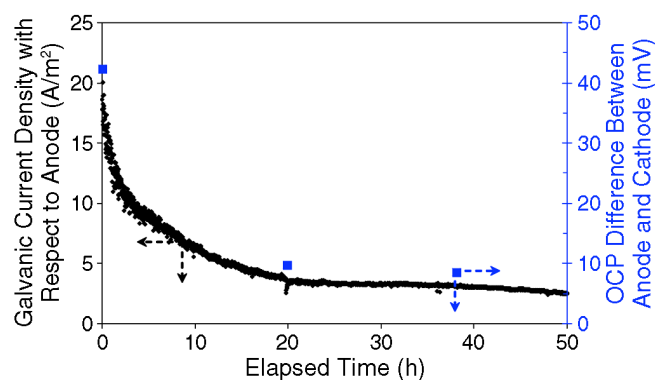


FIGURE 6. Galvanic current density calculated with respect to anode (line) and OCP difference between anode and cathode (points) with time at pH 5.9, $T = 80^\circ\text{C}$, $SS_{\text{FeCO}_3} = 0.8$ to 4, shallow pit, $[\text{NaCl}] = 1$ wt%, mildly agitated solution by a magnetic stirring bar at 500 rpm.

investigate if propagation of localized CO_2 corrosion of mild steel will occur only in the so-called gray zone. In other words, it is assumed that when the supersaturation with respect to FeCO_3 is high ($SS_{\text{FeCO}_3} \gg 1$), the FeCO_3 will precipitate on all the surfaces causing any active pits to “heal.” Conversely, if the solution is highly undersaturated ($SS_{\text{FeCO}_3} \ll 1$), then the FeCO_3 layer on the cathode will dissolve, the driving force for galvanic corrosion will disappear, and uniform corrosion will prevail. Consequently, only when the solution is near the saturation point with respect to FeCO_3 and is therefore in the gray zone, the protective layer will neither dissolve from the cathode nor will it form on the anode and the galvanic cell will operate steadily.

An example of localized corrosion propagation when the solution conditions are in the gray zone was already shown in Figure 6 where supersaturation for FeCO_3 varied in the range: $SS_{\text{FeCO}_3} = 0.8$ to 4. Another example is shown in Figure 7, where it was controlled in a narrower range: $SS_{\text{FeCO}_3} = 0.3$ to 0.9, i.e., the solution was continuously slightly undersaturated with

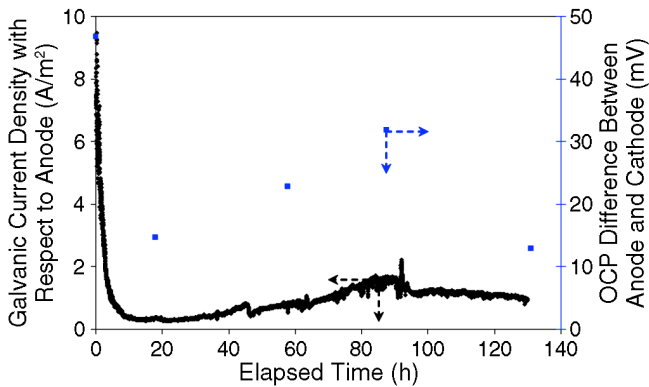


FIGURE 7. Galvanic current density calculated with respect to anode (line) and OCP difference between anode and cathode (points) with time when solution is in the gray zone, i.e., $SS_{\text{FeCO}_3} = 0.3$ to 0.9 , at $T = 80^\circ\text{C}$, $p_{\text{CO}_2} = 0.53$ bar, $\text{pH} 5.9$ to 6.1 , $[\text{NaCl}] = 1$ wt%, stagnant, shallow pit.

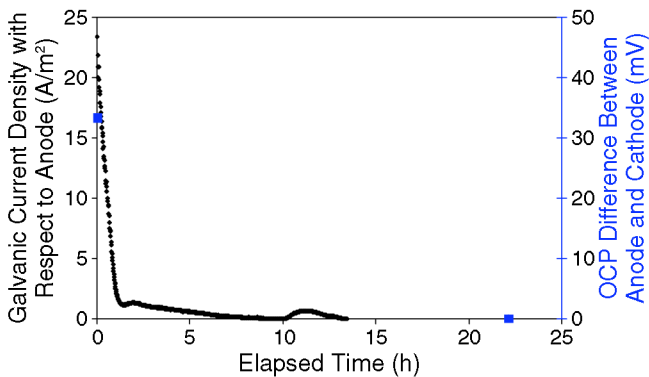


FIGURE 9. Galvanic current density calculated with respect to the anode (line) and OCP difference between anode and cathode (points) with time when solution is not in the gray zone, i.e., the solution is supersaturated: $SS_{\text{FeCO}_3} = 3$ to 9 , at $T = 80^\circ\text{C}$, $p_{\text{CO}_2} = 0.53$ bar, $\text{pH} 5.6$, $[\text{NaCl}] = 1$ wt%, stagnant.

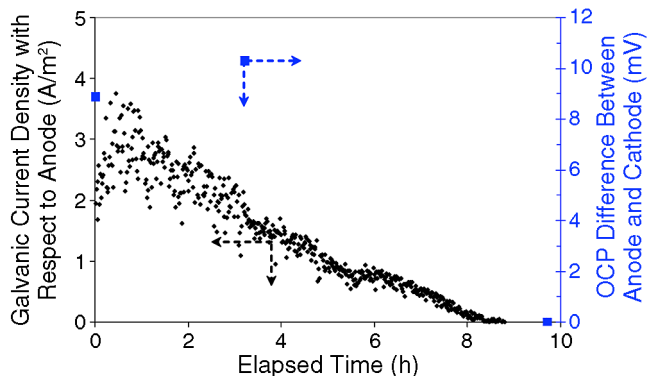


FIGURE 10. Galvanic current density calculated with respect to the anode (line) and OCP difference between anode and cathode (points) with time when solution is not in the gray zone, i.e., the solution is undersaturated: $SS_{\text{FeCO}_3} = 0.2$ to 0.5 , at $T = 80^\circ\text{C}$, $p_{\text{CO}_2} = 0.53$ bar, $\text{pH} 5.8$, $[\text{NaCl}] = 1$ wt%, solution is mildly stirred by a magnetic bar at 100 rpm.

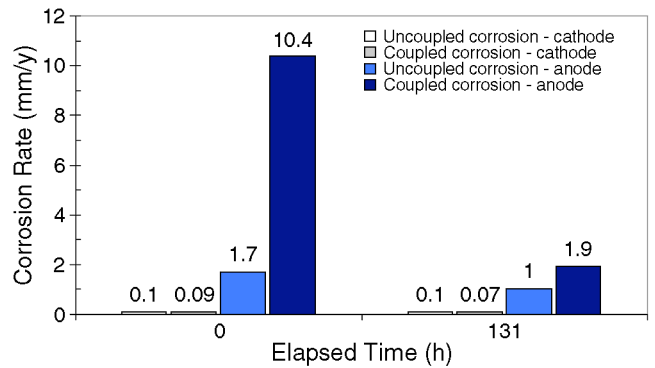


FIGURE 8. Uniform corrosion rates for an uncoupled FeCO_3 -covered cathode and a bare steel anode vs. the localized corrosion rate seen on a coupled anode at the beginning and end of the artificial pit test conducted in the gray zone: $SS_{\text{FeCO}_3} = 0.3$ to 0.9 , at $T = 80^\circ\text{C}$, $p_{\text{CO}_2} = 0.53$ bar, $\text{pH} 5.9$ to 6.1 , $[\text{NaCl}] = 1$ wt%, shallow pit, stagnant.

respect to FeCO_3 . In both cases, the galvanic current was very high initially and then stabilized at a lower value as time progressed.

To put the magnitude of this galvanic current into perspective, it is converted into a corrosion rate and factored into the uncoupled corrosion rates of the anode and cathode. The various corrosion rates of anode and cathode are compared in Figure 8. Clearly, the corrosion rate of the large cathode remains virtually unaffected by the coupling, while the corrosion rate of the coupled anode is doubled.

One situation when the solution is not in the gray zone is depicted in Figure 9. In this case, the FeCO_3 supersaturation is maintained high ($SS_{\text{FeCO}_3} = 3$ to 9), and the galvanic current density, which starts very high, is rapidly reduced to zero, indicating that initial propagation of localized corrosion is stifled due to protective FeCO_3 layer formation on the anode. In this case the pit “healed” and the corrosion rates on both cathode and anode equalized and remained low (<0.1 mm/y).

Another case operating outside the gray zone is shown in Figure 10. When FeCO_3 supersaturation is maintained low ($SS_{\text{FeCO}_3} = 0.2$ to 0.5), the galvanic current density also gradually reduces to zero. In this case, it is because the protective FeCO_3 layer on the cathode dissolves (as visually confirmed) and the driving force for the galvanic coupling (potential difference) disappears. Both the anode and the cathode experienced stable, high uniform corrosion rates (>1 mm/y).

In summary, it was confirmed that propagation of localized corrosion of mild steel in CO_2 solutions will occur only when the solution is maintained in the gray zone, i.e., when the conditions are close to saturation with respect to FeCO_3 . Multiple experiments have shown that this practically translates into a criterion: $SS_{\text{FeCO}_3} = 0.5$ to 2 when no significant FeCO_3

TABLE 3
Chemical Reactions for the CO₂ Aqueous Environment⁴⁵⁻⁴⁶

	Reaction	Equilibrium Constant
Carbon dioxide dissolution	$\text{CO}_{2(g)} \xrightleftharpoons{K_{\text{sol}}} \text{CO}_2$	$K_{\text{sol}} = c_{\text{CO}_2}/p_{\text{CO}_2}$
Carbon dioxide hydration	$\text{CO}_2 + \text{H}_2\text{O} \xrightleftharpoons{K_{\text{hy}}} \text{H}_2\text{CO}_3$	$K_{\text{hy}} = c_{\text{H}_2\text{CO}_3}/c_{\text{CO}_2}$
Carbonic acid dissociation	$\text{H}_2\text{CO}_3 \xrightleftharpoons{K_{\text{ca}}} \text{H}^+ + \text{HCO}_3^-$	$K_{\text{ca}} = c_{\text{H}^+}c_{\text{HCO}_3^-}/c_{\text{H}_2\text{CO}_3}$
Bicarbonate anion dissociation	$\text{HCO}_3^- \xrightleftharpoons{K_{\text{bi}}} \text{H}^+ + \text{CO}_3^{2-}$	$K_{\text{bi}} = c_{\text{H}^+}c_{\text{CO}_3^{2-}}/c_{\text{HCO}_3^-}$
Water dissociation	$\text{H}_2\text{O} \xrightleftharpoons{K_{\text{wa}}} \text{H}^+ + \text{OH}^-$	$K_{\text{wa}} = c_{\text{H}^+}c_{\text{OH}^-}$
Ferrous carbonate precipitation	$\text{Fe}^{2+} + \text{CO}_3^{2-} \xrightleftharpoons{K_{\text{sp}}} \text{FeCO}_{3(s)}$	$K_{\text{sp}} = c_{\text{Fe}^{2+}}c_{\text{CO}_3^{2-}}$

dissolution nor additional precipitation is expected and the galvanic cell is stabilized.

Environmental Factors Affecting Propagation of Localized Corrosion

Since FeCO₃ supersaturation (SS_{FeCO₃}) is found to be one of the key factors that determines propagation of localized corrosion when a galvanic cell is established, let us take a closer look at which environmental factors affect it most. SS_{FeCO₃} is defined as the ratio of the concentration product of iron and carbonated ions and the solubility product:

$$\text{SS}_{\text{FeCO}_3} = \frac{[\text{Fe}^{2+}][\text{CO}_3^{2-}]}{K_{\text{sp}}} \quad (1)$$

where [Fe²⁺] is the actual concentration of the iron ion, [CO₃²⁻] is the actual concentration of the carbonate ion, and K_{sp} is the solubility product for FeCO₃. To put it simply, the SS_{FeCO₃} expresses the degree of departure from thermodynamic equilibrium for FeCO₃.

Ferrous ion, Fe²⁺, is a product of iron dissolution and concentrations of [Fe²⁺] can readily be measured. The carbonate ion, CO₃²⁻, is assumed to be in equilibrium with the other carbonic species in solution; one can write [CO₃²⁻] = c_{CO₃²⁻}, where c_{CO₃²⁻} is the equilibrium concentration. It is influenced by the amount of dissolved CO₂, and pH can be readily calculated from simple water chemistry models.⁴⁵⁻⁴⁶ The pertinent chemical reactions and their equilibrium constants are briefly reproduced in Tables 3 and 4 for the convenience of the reader, where K represents the equilibrium constant for a given reaction and c the equilibrium concentration of a given species.

The solubility product (K_{sp}) of FeCO₃ has been the subject of some controversy and many different expressions exist.⁴⁸⁻⁵⁶ Here, the latest equation⁵⁷ that accounts for both the effects of temperature and ionic strength was used:

$$\log K_{\text{sp}} = -59.3498 - 0.041377 \left(\frac{2.1963}{T_K} + 24.5724 \right) \log(T_K) + 2.518 \left(I^{0.5} - 0.657 \right) I \quad (2)$$

TABLE 4

Values of the Equilibrium Constants for the Reactions Listed in Table 3⁴⁵⁻⁴⁶

$K_{\text{sol}} = \frac{1.45}{1.00258} \times 10^{-(2.27+5.65 \times 10^{-3} T_f - 8.06 \times 10^{-6} T_f^2 + 0.075 \times I)}$	mol/bar
$K_{\text{hy}} = 2.58 \times 10^{-3}$	
$K_{\text{ca}} = 387.6 \times 10^{-(6.41-1.594 \times 10^{-3} T_f + 8.52 \times 10^{-6} T_f^2 - 3.07 \times 10^{-5} p - 0.4772 \times I^{0.5} + 0.1180 \times I)}$	molar
$K_{\text{bi}} = 10^{-(10.61-4.97 \times 10^{-3} T_f + 1.331 \times 10^{-5} T_f^2 - 2.624 \times 10^{-5} p - 1.166 \times I^{0.5} + 0.3466 \times I)}$	molar
$K_{\text{wa}} = 10^{-(29.3868-0.0737549 \times T_K + 7.4788 \times T_K^2)}$	molar ²

T_f is the temperature in Fahrenheit, T_K is absolute temperature, I is ionic strength in molar, and p is the pressure in psi.

where T_K is the temperature in Kelvin. Ionic strength (I) is defined as:⁴⁷

$$I = \frac{1}{2} \sum_i (m_i + z_i^2 + m_i - z_i^2) \quad (3)$$

where m_i is the molarity of species i, z_i is the charge of the species i, and the symbol + or - indicates the positive or negative charge carried by an ion. The equilibrium equations listed above can be used to determine the actual concentration of the bicarbonate ion [CO₃²⁻] required for calculation of SS_{FeCO₃}.

By looking at the expression for SS_{FeCO₃} above, it appears that the key factors that affect it are the concentrations of ferrous ion [Fe²⁺] and the bicarbonate ion [CO₃²⁻]. The Fe²⁺ concentration [Fe²⁺] is usually known, and in the field it is typically present in the concentration range of a few ppm (0 to 10 ppm), while in the lab its concentration can be set and controlled to a desired value. Clearly, a large concentration of Fe²⁺ will lead to supersaturation and precipitation of FeCO₃, particularly at higher temperatures (>60°C) when the kinetics is fast. This fact was used in the present study where rapid formation of FeCO₃ layers was enabled by manipulating the concentration of Fe²⁺. On the other hand, the concentration of the bicarbonate ion [HCO₃⁻] is determined primarily by pH and partial pressure of CO₂.

It should be noted that the present analysis relies primarily on thermodynamic considerations. Clearly, the kinetics of FeCO₃ film formation is another important factor that lies beyond the scope of this discussion. While FeCO₃ supersaturation, SS_{FeCO₃}, is one of

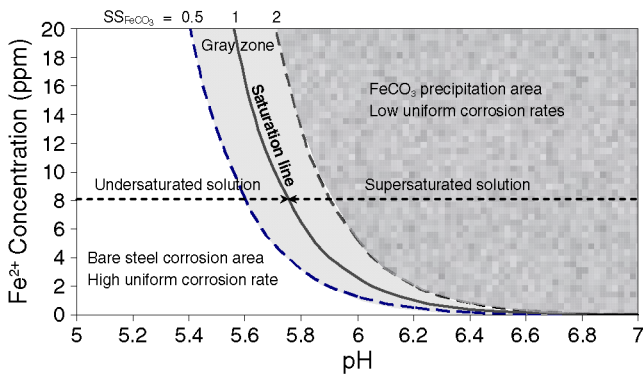


FIGURE 11. Calculated pH effect on solubility of FeCO_3 and the "gray zone" at $T = 80^\circ\text{C}$, $p_{\text{CO}_2} = 0.53$ bar, $[\text{NaCl}] = 1$ wt%.

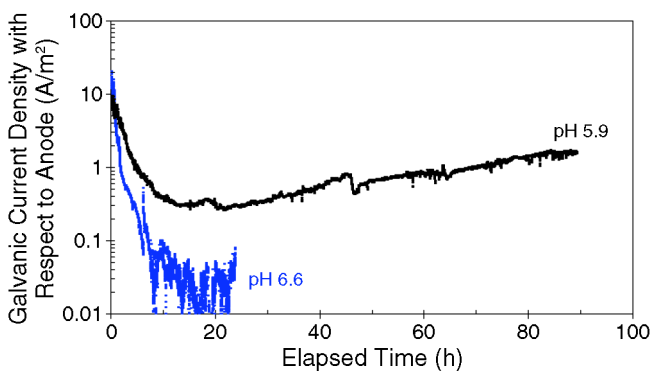


FIGURE 12. Galvanic current density calculated with respect to the anode with time for different pH at $T = 80^\circ\text{C}$, $p_{\text{CO}_2} = 0.53$ bar, $SS_{\text{FeCO}_3} \approx 0.5$ to 4, shallow pit, $[\text{NaCl}] = 1$ wt%, stagnant.

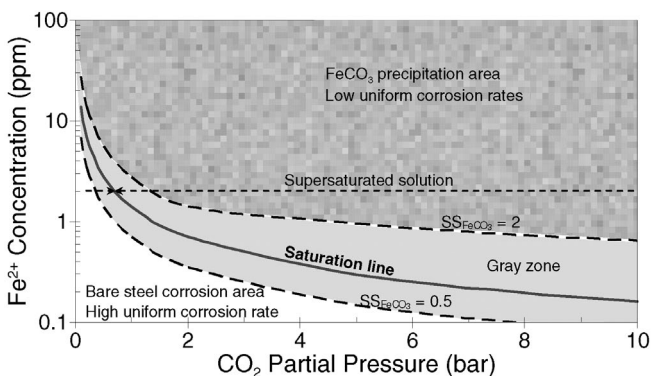


FIGURE 13. Calculated effect of CO_2 partial pressure on solubility of FeCO_3 and the "gray zone" at $T = 80^\circ\text{C}$, pH 6.0, $[\text{NaCl}] = 1$ wt%.

the key factors determining the kinetics, the other one is temperature. Only at high temperature ($>50^\circ\text{C}$) does FeCO_3 form fast enough to overpower the undermining corrosion process and form a protective layer. Therefore, the galvanic mechanism of localized corrosion considered here does not carry over to lower temperatures, and all the experiments in this study were conducted at 80°C .

Effect of pH — As the pH increases (H^+ concentration decreases), the CO_3^{2-} concentration increases, which can be easily understood by inspecting the equilibrium reactions listed in Table 3. In Figure 11, the calculated effect of pH on solubility of FeCO_3 is shown for a given set of operating conditions. Similar graphs for other conditions can be created by solving the equilibrium equations given above. Also in Figure 11, the calculated effect of pH on the gray zone is shown, where propagation of localized corrosion can be expected. Practical limits for the gray zone are taken to be $0.5 < SS_{\text{FeCO}_3} < 2$, as discussed above. If one assumes that the range for Fe^{2+} concentration is 0 to 10 ppm in the field, then under these conditions the graph suggests that it is unlikely to get FeCO_3 precipitation and localized corrosion propagation below pH 5.6. One can judge in this case that the localized attack is possible in the range from pH 5.7 to 6.4. Above pH 6.6, it appears that, for almost any Fe^{2+} concentration, FeCO_3 will precipitate and low uniform corrosion rates will prevail.

This was confirmed by conducting artificial pit tests where all parameters were identical, other than the pH (Figure 12). The first case at pH 5.9, where significant galvanic current and localized corrosion was obtained, was already discussed above. In an identical experiment conducted at pH 6.6, the galvanic current rapidly diminished and no localized corrosion could be observed. Very low general corrosion rates were obtained on both anode and cathode (<0.1 mm/y).

Effect of CO_2 Partial Pressure — The effect of CO_2 partial pressure on solubility of FeCO_3 and indirectly on localized corrosion propagation likelihood can also be deduced by looking at the reaction equilibria presented above. All other conditions being the same, higher partial pressure of CO_2 leads to higher dissolved CO_2 concentration and eventually to higher concentrations of the CO_3^{2-} ion. This means that the solubility of FeCO_3 decreases with increasing partial pressure of CO_2 as shown in Figure 13. It can be seen that at these conditions, FeCO_3 will readily form as the partial pressure of CO_2 exceeds 2 bar for any measurable Fe^{2+} concentration (>1 ppm) and can hardly be avoided at even higher partial pressures of CO_2 . The gray zone conditions can be met practically only in the lower range of partial pressures of CO_2 , which are most common for field conditions (<2 bar). At higher partial pressures of CO_2 the gray zone is feasible only for very low Fe^{2+} concentrations (<1 ppm), giving way to protective FeCO_3 film formation, suggesting a very low likelihood of both uniform and localized attack at these conditions.

Effect of Salt — Another factor that does not appear explicitly in the expression for SS_{FeCO_3} above, but needs to be considered, is the effect of salt (NaCl). Typical concentrations seen in the field brine are 1 wt% to 3 wt% while condensed water seen in wet gas lines

has no salt. However, cases with up to 20 wt% of salt in the brine are not uncommon. In a recent study, no effect of salt on general CO_2 corrosion was found across a broad concentration range. However, a Cl^- ion concentration effect on localized CO_2 corrosion has been reported in the literature,^{16,25,27} with lower pit density¹⁶ and higher localized corrosion rate^{25,27} observed at higher NaCl concentration. In the first approximation, the effect of salt can be included in this analysis by looking at the effect it has on reaction equilibria shown above, by considering a change in ionic strength of the solution. This is summarized in Figure 14, where the calculated effect of NaCl concentration on the solubility of FeCO_3 and the gray zone is shown, for a given set of operating conditions. It can be seen that the solubility of FeCO_3 increases with increasing salt concentration, making it more difficult to form protective FeCO_3 layers. Interestingly, it also shows that the “gray zone” widens as the salt concentration increases, making it more likely to get localized corrosion propagation as the concentration of NaCl increases.

To verify this observation, a series of AP tests were conducted at various salt concentrations. The results are summarized in Figure 15, where a significant effect of salt concentration on the galvanic current is evident. The highest localized attack was obtained for the highest NaCl concentration. No localized attack was obtained for the lowest NaCl concentration, what could also be attributed, in part, to the lower conductivity of the solution.

Effect of Flow — Fluid flow was already mentioned as one of the key factors in initiation of localized CO_2 corrosion of mild steel. In this study, the focus is on localized corrosion propagation and the role of mixing introduced by turbulent flow. To study this effect, another series of tests was conducted with vigorous stirring using a rotating magnet (at 500 rpm) and the results were compared with the stagnant test in the same environment. It is recognized here that this is not the best way to introduce controlled flow conditions; however, it was the only way easily achievable given the constraints of the equipment used. The galvanic current densities comparison (stagnant vs. 500 rpm) are depicted in Figure 16. A significant increase in the galvanic current density under stirred flow condition is observed (although the effect seems to diminish over time). The large difference in the galvanic current can be explained easily by the fact that any accumulation of corrosion products on the anode was minimized by the flow, because of turbulent mixing sweeping away any corrosion products generated in the vicinity of the anode and thereby stabilizing the galvanic cell.

In another series of tests, the anode was recessed within the cathode by 2 mm, to create a quiet environment shielded from the bulk flow, which was agitated by the rotating magnet. These results are compared

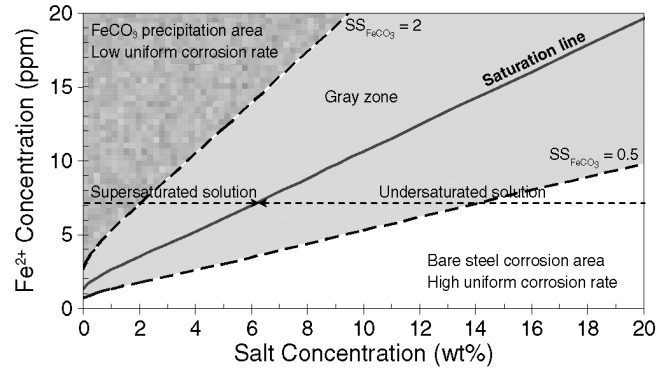


FIGURE 14. Salt effect on the “gray zone” width at $T = 80^\circ\text{C}$, $p_{\text{CO}_2} = 0.53$ bar, $\text{pH} 6.0$, $[\text{NaCl}] = 1$ wt%.

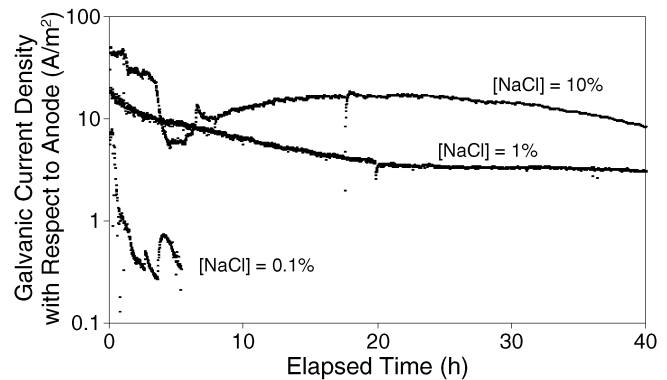


FIGURE 15. Galvanic current density calculated with respect to the anode for different NaCl concentrations at $\text{pH} 5.9$ to 6.0 , $T = 80^\circ\text{C}$, shallow pit, $SS_{\text{FeCO}_3} = 0.2$ to 4 , stirring speed = 400 rpm.

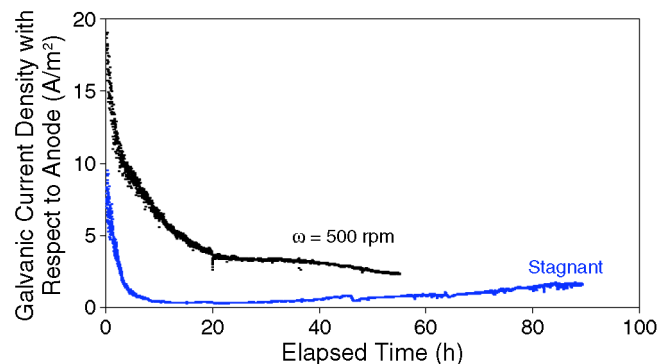


FIGURE 16. Galvanic current density calculated with respect to the anode for a stagnant and stirred solution using a rotating magnet at $\text{pH} 5.8$ to 5.9 , $SS_{\text{FeCO}_3} = 0.3$ to 4 , $T = 80^\circ\text{C}$, shallow pit, $[\text{NaCl}] = 1$ wt%.

with others obtained in experiments conducted under similar conditions in Figure 17. As expected, the recessed pit behaved similarly to a shallow pit under stagnant condition.

In summary, these results indicate that once a bare steel surface is exposed to turbulent flow, localized corrosion propagation proceeds very fast initially,

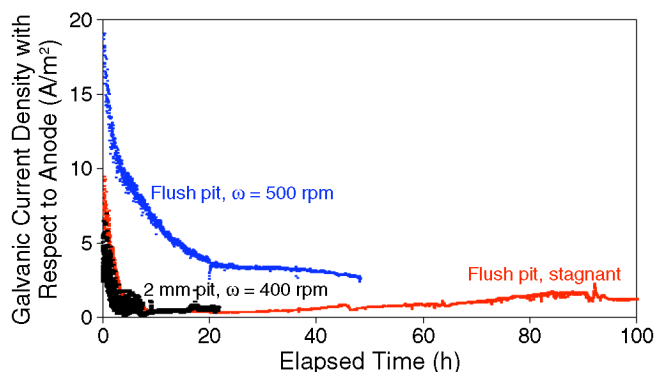


FIGURE 17. Galvanic current density calculated with respect to the anode for a receded pit (depth = 2 mm) and shallow pit (depth <0.1 mm) at pH 5.8 to 5.9, $T = 80^{\circ}\text{C}$, $SS_{\text{FeCO}_3} = 0.2$ to 4 [NaCl] = 1 wt%.

due to a galvanic coupling with the FeCO_3 -covered surface. However, as the pit recedes, the propagation rate slows down due to mass-transfer limitations. At some point, the propagation may stop altogether if protective FeCO_3 reforms on the steel surface. Conversely, if flow and water chemistry conditions remain favorable, rapid pit propagation may continue until the point of line failure.

CONCLUSIONS

- ❖ Localized CO_2 corrosion propagates when a stable difference in corrosion potential is established between a larger-area mild steel surface covered by a protective FeCO_3 layer and a smaller-area bare steel surface corresponding to a bottom of a pit or a mesa corrosion surface.
- ❖ Stable propagation of localized corrosion of mild steel in CO_2 solutions will occur only when the solution is maintained in the gray zone, i.e., when the conditions are close to saturation with respect to FeCO_3 . This practically translates into a situation where for $SS_{\text{FeCO}_3} = 0.5$ to 2, no significant FeCO_3 dissolution or additional precipitation is expected and the galvanic cell is stabilized.
- ❖ Key environmental factors that affect propagation of localized CO_2 corrosion of mild steel are temperature, pH, partial pressure of CO_2 , salt concentration, and flow velocity.
- ❖ Only at high temperature ($>50^{\circ}\text{C}$) does FeCO_3 form fast enough to overpower the undermining corrosion process and form a protective layer. Therefore, the galvanic mechanism of localized corrosion is only valid in the higher temperature range, where protective FeCO_3 layers form.
- ❖ Localized CO_2 attack due to galvanic coupling is only possible in the pH range when moderately protective FeCO_3 layers form, typically pH 5.5 to pH 6.5. Above pH 6.5, it appears that, for almost any Fe^{2+} concentration, FeCO_3 will precipitate and low uniform corrosion rates will prevail. Conversely, at pH lower

than 5.5, protective FeCO_3 is unlikely to form and high uniform corrosion rates are to be expected.

- ❖ The solubility of FeCO_3 decreases with increasing partial pressure of CO_2 . For partial pressures of CO_2 significantly higher than 2 bar, very protective FeCO_3 films form at high temperature, suggesting a very low likelihood of both uniform and localized attack. In the lower range of partial pressures of CO_2 (between 0.1 bar and 2 bar), which are most common for field conditions, the likelihood of localized attack is highest given that the other conditions are favorable.

- ❖ Solubility of FeCO_3 increases with increasing salt concentration, making it more difficult to form protective FeCO_3 layers and more likely to get localized corrosion propagation.

- ❖ Turbulent flow assists localized corrosion propagation by sweeping away corrosion products from the rapidly corroding steel surface and thereby preventing reformation of the protective FeCO_3 layer.

- ❖ Pit propagation proceeds initially very fast, due to a galvanic coupling with the FeCO_3 -covered surface. However, as the pit recedes, the propagation rate slows down and is governed by mass-transfer limitations. At some point, the propagation may stop if protective FeCO_3 re-forms on the steel surface. Conversely, if flow and water chemistry conditions remain favorable, rapid pit propagation may continue until the point of line failure.

ACKNOWLEDGMENTS

Helpful discussions with D. Young are much appreciated as well as his help with the many revisions of the paper. The assistance to fabricate the artificial pit came from J. Addis. The authors also appreciate the financial support from the Corrosion Center Joint Industry Project advisory board members, namely, Baker Petrolite, BP, Champion Technologies, Chevron, Clariant, Columbia Gas Transmission, ConocoPhillips, Eni, ExxonMobil, MI Production Chemicals, Nalco, Occidental Oil Company, Petrobras, PTTEP, Saudi Aramco, Shell, Tenaris, and Total.

REFERENCES

1. M.W. Joosten, T. Johnsen, H.H. Hardy, J. Jossang, J. Feder, "Fractal Behavior of CO_2 Pits," CORROSION/92, paper no. 406 (Houston, TX: NACE International, 1992).
2. M.W. Joosten, T. Johnsen, A. Dugstad, T. Walmann, J. Jossang, P. Meakin, J. Feder, "In Situ Observation of Localized CO_2 Corrosion," CORROSION/94, paper no. 3 (Houston, TX: NACE, 1994).
3. K. Videm, A. Dugstad, *Mater. Perform.* 28, 3 (1989): p. 63.
4. K. Videm, A. Dugstad, *Mater. Perform.* 28, 4 (1989): p. 46.
5. K. Videm, A.M. Koren, "Corrosion, Passivity, and Pitting of Carbon Steel in Aqueous Solutions of HCO_3^- , CO_2 , and Cl^- ," CORROSION/92, paper no. 12 (Houston, TX: NACE, 1992).
6. K. Videm, "Fundamental Studies Aimed at Improving Models for Prediction of CO_2 Corrosion of Carbon Steels," Progress in the Understanding and Prevention of Corrosion, vol. 1, 10th European Corrosion Congress, eds. J.M. Costa, A.D. Mercer (London, U.K.: Institute of Materials for the Sociedad Espanola de Quimica on behalf of European Federation of Corrosion, 1993), p. 504-512.

7. A. Marie, K. Halvorsen, T. Søntvedt, "CO₂ Corrosion Model for Carbon Steel Including a Wall Shear Stress Model for Multiphase Flow and Limits for Production to Avoid Mesa Attack," CORROSION/99, paper no. 42 (Houston, TX: NACE, 1999).
8. M.H. Achour, J. Kolts, A.H. Johannes, G. Liu, "Mechanistic Modeling of Pit Propagation in CO₂ Environment Under High Turbulence Effects," CORROSION/93, paper no. 87 (Houston, TX: NACE, 1993).
9. S. Nešić, Y. Xiao, B.F.M. Pots, "A Quasi 2-D Localized Corrosion Model," CORROSION/2004, paper no. 628 (Houston, TX: NACE, 2004).
10. G. Schmitt, W. Bucken, R. Fanebust, *Corrosion* 48, 5 (1991): p. 431.
11. G. Schmitt, M. Horstemeier, "Fundamental Aspects of CO₂ Metal Loss Corrosion—Part II: Influence of Different Parameters on CO₂ Corrosion Mechanism," CORROSION/2006, paper no. 06112 (Houston, TX: NACE, 2006).
12. G. Schmitt, T. Gudde, E. Strobel-Effertz, "Fracture Mechanical Properties of CO₂ Corrosion Product Layers and Their Relation to Localized Corrosion," CORROSION/96, paper no. 9 (Houston, TX: NACE, 1996).
13. G. Schmitt, C. Bosch, U. Pankoke, W. Bruckhoff, G. Siegmund, "Evaluation of Critical Flow Intensities for FILC in Sour Gas Production," CORROSION/98, paper no. 46 (Houston, TX: NACE, 1998).
14. G. Schmitt, M. Mueller, M. Papenfuss, E. Strobel-Effertz, "Understanding Localized CO₂ Corrosion of Mild Steel from Physical Properties of FeCO₃ Layers," CORROSION/99, paper no. 38 (Houston, TX: NACE, 1999).
15. G. Schmitt, M. Mueller, "Critical Wall Shear Stresses in CO₂ Corrosion of Carbon Steel," CORROSION/2002, paper no. 44 (Houston, TX: NACE, 2002).
16. G. Schmitt, S. Feinen, "Effect of Anions and Cations on the Pit Initiation in CO₂ Corrosion of Iron and Steel," CORROSION/2000, paper no. 00001 (Houston, TX: NACE, 2000).
17. G. Schmitt, C. Bosch, P. Plagemann, K. Moeller, "Local Wall Shear Stress Gradients in the Slug Flow Regime—Effect of Hydrocarbon and Corrosion Inhibitor," CORROSION/2002, paper no. 02244 (Houston, TX: NACE, 2002).
18. C.F. Chen, M.X. Lu, D.B. Sun, Z.H. Zhang, W. Chang, *Corrosion* 61, 6 (2005): p. 594.
19. Z. Xia, K.-C. Chou, Z. Szklarska-Smialowska, *Corrosion* 45, 8 (1989): p. 636.
20. J.-L. Crolet, "Which CO₂ Corrosion, Hence Which Prediction?" in *Predicting CO₂ Corrosion in the Oil and Gas Industry*, European Federation of Corrosion publication no. 13 (London, U.K.: The Institute of Materials, 1994), p. 1-26.
21. R. Nyborg, A. Dugstad, "Mesa Corrosion Attack in Carbon Steel and 0.5% Chromium Steel," CORROSION/98, paper no. 29 (Houston, TX: NACE, 1998).
22. A. Dugstad, "Mechanism of Protective Film Formation During CO₂ Corrosion of Carbon Steel," CORROSION/98, paper no. 31 (Houston, TX: NACE, 1998).
23. R. Nyborg, "Initiation and Growth of Mesa Corrosion Attack During CO₂ Corrosion of Carbon Steel," CORROSION/98, paper no. 48 (Houston, TX: NACE, 1998).
24. R. Nyborg, A. Dugstad, "Understanding and Prediction of Mesa Corrosion," CORROSION/2003, paper no. 03642 (Houston, TX: NACE, 2003).
25. Y. Sun, K. George, S. Nešić, "The Effect of Cl⁻ and Acetic Acid on Localized CO₂ Corrosion in Wet Gas Flow," CORROSION/2003, paper no. 03327 (Houston, TX: NACE, 2003).
26. Y. Sun, S. Nešić, "A Parametric Study and Modeling on Localized CO₂ Corrosion in Horizontal Wet Gas Flow," CORROSION/2004, paper no. 04380 (Houston, TX: NACE, 2004).
27. Y. Sun, "Localized CO₂ Corrosion in Horizontal Wet Gas Flow" (Ph.D. diss., Ohio University, 2003).
28. J. Han, Y. Yang, B. Brown, S. Nešić, "Electrochemical Investigation of Localized CO₂ Corrosion on Mild Steel," CORROSION/2007, paper no. 07323 (Houston, TX: NACE, 2007).
29. J. Han, Y. Yang, B. Brown, S. Nešić, "Roles of Passivation and Galvanic Effects in Localized CO₂ Corrosion of Mild Steel," CORROSION/2008, paper no. 08332 (Houston, TX: NACE, 2008).
30. J. Han, D. Young, S. Nešić, "Characterization of the Passive Film on Mild Steel in CO₂ Environments," ICC/2008, paper no. 2511 (Houston, TX: NACE, 2008).
31. J. Han, S. Nešić, B.N. Brown, "Galvanic Model for Localized CO₂ Corrosion," ICC/2008, paper no. 2687 (Houston, TX: NACE, 2008).
32. J. Han, D. Young, H. Colijn, A. Tripathi, S. Nešić, *Ind. Eng. Chem. Res.* 48, 13 (2009): p. 6296-6302.
33. J. Marsh, T. The, S. Ounnas, M. Richardson, "Corrosion Management for Aging Pipelines—Experience from the Forties Field," 2008 SPE International Oilfield Corrosion Conf., paper no. SPE 114141 (Richardson, TX: SPE International, 2008).
34. U.R. Evans, *An Introduction to Metallic Corrosion*, 3rd ed. (London, U.K.: Edward Arnold Publisher, Ltd., 1981), p. 36.
35. D.A. Jones, *Principles and Prevention of Corrosion*, 2nd ed. (Upper Saddle River, NJ: Prentice Hall, Inc., 1996), p. 191.
36. D.D. Macdonald, M. Urquidi-Macdonald, *J. Electrochem. Soc.* 137, 8 (1990): p. 2395-2402.
37. D.D. Macdonald, *J. Electrochem. Soc.* 139, 12 (1992): p. 3434-3449.
38. A. Turnbull, D. Coleman, A.J. Griffiths, P.E. Francis, L. Orkney, *Corrosion* 59, 3 (2003): p. 250.
39. J. Marsh, J.W. Palmer, R.C. Newman, "Evaluation of Inhibitor Performance for Protection Against Localized Corrosion," CORROSION/2002, paper no. 288 (Houston, TX: NACE, 2002).
40. J. Amri, E. Gulbrandsen, R.P. Nogueira, *Electrochem. Comm.* 10, 2 (2008): p. 200-203.
41. J. Amri, E. Gulbrandsen, R.P. Nogueira, *Electrochim. Acta* 54, 28 (2009): p. 7338-7344.
42. Y. Tan, Y. Fwu, K. Bhardwaj, S. Bailey, R. Gubner, "Review of Critical Issues in Carbon Dioxide Corrosion Testing and Monitoring Techniques," CORROSION/2010, paper no. 10155 (Houston, TX: NACE, 2010).
43. K. Lepková, R. Gubner, "Development of Standard Test Method for Investigation of Under-Deposit Corrosion in Carbon Dioxide Environment and Its Application in Oil and Gas Industry," CORROSION/2010, paper no. 10331 (Houston, TX: NACE, 2010).
44. K. Chokshi, W. Sun, S. Nešić, "FeCO₃ Layer Growth and the Effect of Inhibition in CO₂ Corrosion of Mild Steel," CORROSION/2005, paper no. 05285 (Houston, TX: NACE, 2005).
45. M. Nordsveen, S. Nešić, R. Nyborg, A. Stangeland, *Corrosion* 59, 5 (2003): p. 443.
46. S. Nešić, M. Nordsveen, R. Nyborg, A. Stangeland, "A Mechanistic Model for CO₂ Corrosion with Protective FeCO₃ Films," CORROSION/2001, paper no. 01040 (Houston, TX: NACE, 2001).
47. T. Engel, P. Reid, *Thermodynamics, Statistical Thermodynamics, and Kinetics* (San Francisco, CA: Pearson, 2006), p. 230.
48. J. Bruno, P. Wersin, W. Stumm, *Geochim. Cosmochim. Acta* 56 (1992): p. 1149-1155.
49. J. Greenberg, M. Tomson, *Appl. Geochem.* 7 (1992): p. 185.
50. A. Dugstad, "The Importance of FeCO₃ Supersaturation on the CO₂ Corrosion of Carbon Steels," CORROSION/92, paper no. 14 (Houston, TX: NACE, 1992).
51. W. Preis, H. Gamsjäger, *Monatsh. Chem.* 132 (2001): p. 1327-1346.
52. D.L. Jensen, J.K. Boddum, J.C. Tjell, T.H. Christensen, *Appl. Geochem.* 17 (2002): p. 503.
53. W. Preis, H. Gamsjäger, *Phys. Chem. Chem. Phys.* 4 (2002): p. 4014.
54. C.A.R. Silva, X. Liu, F.J. Millerol, *J. Solution Chem.* 31, 2 (2002): p. 97.
55. G.M. Marion, D.C. Catling, J.S. Kargel, *Geochim. Cosmochim. Acta* 67, 2 (2003): p. 4251.
56. S. Nešić, Corrosion Center, Ohio University, personal communication, 2007.
57. W. Sun, S. Nešić, D. Young, R. Woollam, *Ind. Eng. Chem. Res.* 47, 5 (2008): p. 1738.